Numerical Solution to Boussinesq-Type Equation in Microstructured Solids

Master thesis

Student: Mohammad Ali Afzal

Student code: 177252YAFM

Supervisor: Arkadi Berezovski

Study program: Applied Physics

Tallinn 2025

TALLINNA TEHNIKAÜLIKOOL

Loodusteaduskond

Boussinesq-tüüpi võrrandi arvuline lahendus mikrostruktureeritud tahkistes

Magistritöö

Üliõpilane: Mohammad Ali Afzal

Üliõpilaskood: 177252YAFM

Juhendaja: Arkadi Berezovski

Õppekava: Rakendusfüüsika

Tallinn 2025

Author’s declaration

I hereby declare that I have written this thesis independently and the thesis has not previously been submitted for defence. All works and major viewpoints of the other authors, data from sources of literature and elsewhere used for writing this paper have been properly cited.

Thesis author’s name: Mohammad Ali Afzal

Signature:

Date:

Supervisor’s resolution

The thesis complies with the requirements for Master’s theses.

Supervisor: Arkadi Berezovski

Signature:

Date:

Abstract

This thesis presents a numerical study of the Boussinesq-type equation in microstructured solids using the finite volume method. The work begins with the classical Good Boussinesq equation, highlighting the interaction between nonlinearity and dispersion responsible for the formation of solitons. Analytical one- and two-soliton solutions are highlighted to provide benchmark comparisons for numerical validation. The developed finite volume scheme, based on local equilibrium and excess-quantity formulations, accurately captures soliton propagation, collision, and recovery with small L^2 errors.

The Boussinesq equation is further extended by incorporating internal variables to represent microstructural effects. This addition modifies the effective dispersion coefficient while maintaining the nonlinear framework of the equation. Numerical experiments show that internal variables change the soliton profile and influence phase behavior, indicating enhanced dispersive localization due to microstructure.

The proposed method demonstrates robustness, accuracy, and physical consistency, making it a reliable tool for analyzing nonlinear wave propagation in both classical and microstructured continua.

Keywords: Boussinesq-type equation, finite volume method, soliton, microstructure, dispersion, nonlinear waves.

Kokkuvõte

Käesolevas magistritöös on esitatud arvuline uurimus Boussinesq-tüüpi võrrandi kohta mikrostruktureeritud tahkistes, kasutades lõplike ruumimahtude meetodit. Töö algab klassikalise Good'i Boussinesqi võrrandi käsitlemisega, rõhutades mittelineaarsuse ja dispersiooni vastastikust mõju, mis põhjustab solitonide teket. Ühe- ja kahesolitonilised analüütilised lahendused on esile tõstetud, et kasutada neid võrdluseks arvulise valideerimise eesmärgil. Välja töötatud lõplike ruumimahtude skeem, mis põhineb lokaalse tasakaalu ja liigsete suuruste kontseptsioonil, kirjeldab täpselt solitoni levikut, kokkupõrget ja taastumist väikeste L^2-vigadega.

Boussinesqi võrrandit on laiendatud sisemiste muutujate lisamisega, et kirjeldada mikrostruktuuri mõju materjalis. See täiendus muudab efektiivset dispersioonitegurit, säilitades samas võrrandi mittelineaarse struktuuri. Arvulised katsed näitavad, et sisemised muutujad muudavad solitoni profiili ja mõjutavad faasikäitumist, viidates mikrostruktuurist tingitud dispersiooni lokaliseerumise tugevnemisele.

Välja pakutud meetod on stabiilne, täpne ja füüsikaliselt järjekindel, pakkudes usaldusväärset tööriista mittelineaarsete lainete leviku uurimiseks nii klassikalistes kui ka mikrostruktureeritud keskkondades.

Võtmesõnad: Boussinesq-tüüpi võrrand, lõplike ruumimahtude meetod, soliton, mikrostruktuur, dispersioon, mittelineaarsed lained.

Contents

List of figures

List of tables

1 Boussinesq Equation

Wave propagation in elastic and microstructured solids is an essential topic in applied physics and engineering, with applications ranging from non-destructive testing to advanced materials design. The classical wave equation, while useful, is often insufficient to capture complex behaviours in such materials, particularly when both nonlinear effects and dispersive effects are significant. The Boussinesq-type equation, originally derived in the context of shallow water waves, has since been extended and adapted for use in a broad range of physical systems, including nonlinear elastic media, lattice structures, and microstructured solids (Whitham, 1974; Bona, Chen, & Saut, 2002; Drazin & Johnson, 1989).

1.1 Historical and Physical Background

The Boussinesq equation was first introduced in the 1870s by Joseph Boussinesq to describe long surface waves in shallow water. Since then, it has evolved into a family of nonlinear partial differential equations used to model wave propagation in dispersive media. In its classical form, the Boussinesq equation incorporates both a second-order time derivative (representing wave propagation) and higher-order spatial derivatives (accounting for dispersion). When applied to solids, especially those with internal structure or characteristic length scales, the Boussinesq-type equation serves as a refined model that includes micro-inertial and dispersive effects (Whitham, 1974).

In modern continuum mechanics, Boussinesq-type equations are often derived from homogenization or asymptotic methods applied to discrete lattice models or microstructured continua. They are particularly effective in modeling solitary wave propagation, or solitons, which are localized, nonlinear wave structures that maintain their shape during travel and interaction— a feature not captured by purely linear models (Drazin & Johnson, 1989; Maugin, 1999).

1.2 General Form of the Boussinesq-Type Equation

The normalized Good Boussinesq equation, which ensures well-posedness and stability, is given by (Christov et al., 1996):

$$u_{tt} - u_{xx} + \beta(u^2)_{xx} + \alpha u_{xxxx} = 0, \tag{1.1}$$

where:

- $u(x,t)$ represents the wave displacement.
- α is the dispersion coefficient, responsible for high-order spatial corrections.
- β is the nonlinearity coefficient, responsible for amplitude-dependent effects.

This form is often referred to as the Good Boussinesq equation due to the stabilizing positive coefficient in the highest-order derivative term. In contrast, the Bad Boussinesq equation, which differs only by the sign of the u_{xxxx} term, is known to be ill-posed and prone to numerical instabilities (Manoranjan et al., 1984).

1.3 Role of Dispersion and Nonlinearity

The interplay between nonlinearity and dispersion in the Boussinesq equation is central to the formation of stable wave structures such as solitons:

- The dispersive term αu_{xxxx} causes wave packets to spread, mimicking the effects of internal structure or microinertia in a solid (Achenbach, 1973).
- The nonlinear term $\beta(u^2)_{xx}$ causes wave steepening, allowing localized pulses to form.

It is the balance between these two mechanisms—nonlinearity focusing the wave and dispersion spreading it—that enables the existence of soliton solutions, which are stable, non-decaying waveforms (Dutykh & Clamond, 2016).

1.4 Applications and Soliton Relevance

Boussinesq-type models are used across physics and engineering to describe:

- Surface and internal waves in shallow water (Bona et al., 2002)
- Elastic wave propagation in nonlinear solids (Achenbach, 1973)
- Longitudinal waves in molecular chains and DNA strands (Bona et al., 2002)
- Optical pulse propagation in nonlinear media (Bona et al., 2002)

A particularly interesting class of solutions are solitons—localized waves that can interact nonlinearly and still retain their shape and velocity (Drazin, 1989; Dutykh & Clamond, 2016). Solitons are of great theoretical and practical importance: in physics, they model particle-like phenomena; in engineering, they allow for robust waveguides and signal transmission systems (LeVeque, 2002; Sjölander, 2021).

In this thesis, we focus on simulating one and two-soliton solutions of the Good Boussinesq equation using a finite volume method in microstructured solids. The goal is to numerically capture soliton propagation and interaction, validate the correctness of the scheme, and compare the results against exact analytical solutions.

2 Analytical Solution of the Good Boussinesq Equation

Soliton solutions play a central role in the study of nonlinear dispersive wave equations such as the Boussinesq equation (Almatrafi et al., 2020; Ablowitz & Segur, 1981). These solutions represent localized wave packets that maintain their shape and speed over time, even after interacting with other solitons. In the context of this thesis, analytical soliton solutions serve as precise reference benchmarks for validating the accuracy of the numerical scheme implemented for solving the Boussinesq-type equation in microstructured solids.

2.1 Traveling Wave Ansatz

To derive a soliton solution analytically, we assume a traveling wave solution of the form (Christov et al., 1996):

$$u(x,t) = f(\xi), \text{where } \xi = x - ct, \tag{2.1}$$

where:

- c is the wave velocity.
- $f(\xi)$ is a function of ξ that we will determine.
- This assumption reduces the partial differential equation (PDE) to an ordinary differential equation (ODE).

Using the chain rule (Bona et al., 1985), derivatives transform as:

$$\frac{\partial u}{\partial t} = -c\frac{df}{d\xi}, \qquad \frac{\partial^2 u}{\partial t^2} = c^2\frac{d^2 f}{d\xi^2}, \tag{2.2}$$

$$\frac{\partial u}{\partial x} = \frac{df}{d\xi}, \qquad \frac{\partial^2 u}{\partial x^2} = \frac{d^2 f}{d\xi^2}, \qquad \frac{\partial^4 u}{\partial x^4} = \frac{d^4 f}{d\xi^4}. \tag{2.3}$$

Substituting these derivatives into the "Good" Boussinesq equation:

$$c^2 f'' - f'' + \beta(2ff'') + \alpha f^{(4)} = 0, \tag{2.4}$$

$$(c^2 - 1)f'' + 2\beta ff'' + \alpha f^{(4)} = 0. \tag{2.5}$$

To simplify, integrate once with respect to ξ (assuming vanishing conditions at infinity):

$$(c^2 - 1)f' + \beta(f^2)' + \alpha f''' = 0, \tag{2.6}$$

$$(c^2 - 1)f + \beta f^2 + \alpha f'' = 0. \tag{2.7}$$

This is a second-order ODE, and it admits the exact bell-shaped soliton solution (Debnath, 1997; Ablowitz & Segur, 1981):

$$f(\xi) = A \cdot \operatorname{sech}^2(\kappa\xi). \tag{2.8}$$

2.2 One-Soliton Solution

Substituting the soliton form (Eq. 2.8) into the ordinary differential equation (Eq. 2.7) and comparing coefficients gives the expressions for the amplitude A and inverse width κ (Bona et al., 1985):

$$A = \frac{3(c^2-1)}{2\beta}, \qquad \kappa = \sqrt{\frac{(c^2-1)}{4\alpha}}. \tag{2.9}$$

Thus, the full 1-soliton solution is:

$$u(x,t) = \frac{3(c^2-1)}{2\beta} \cdot \operatorname{sech}^2\left(\sqrt{\frac{(c^2-1)}{4\alpha}}(x - ct - x_0)\right). \tag{2.10}$$

This solution describes a wave centered at $x = x_0 + ct$ with amplitude and width determined by the dispersion (α) and nonlinearity (β) coefficients.

2.3 Two Solitons Solution

An analytical expression for the two-soliton solution is more complex but can be derived using Hirota's bilinear method (Hirota, 1971). For numerical testing purposes, a common approach is to construct two non-interacting solitons at t = 0, placed far enough apart so that their interaction is negligible.

We use:

$$u(x,0) = u_1(x) + u_2(x), \tag{2.11}$$

$$u_1(x) = A \cdot \operatorname{sech}^2\left(\kappa\left(x - x_{0,1}\right)\right), \qquad u_2(x) = A \cdot \operatorname{sech}^2\left(\kappa\left(x - x_{0,2}\right)\right), \tag{2.12}$$

with corresponding velocities:

$$w(x,0) = -c \cdot u_1(x) + c \cdot u_2(x). \tag{2.13}$$

This initial condition results in two solitons traveling in opposite directions. As shown later in the numerical section, the solitons interact and pass through each other —restoring their shape and speed after the collision, a hallmark of solitonic behaviour (Dutykh & Clamond, 2016).

2.4 Soliton Properties

The analytical soliton solution has several key features (Drazin, 1989; Dutykh & Clamond, 2016):

- Shape preservation: The sech² profile remains unchanged over time.
- Amplitude-speed relation: Larger-amplitude solitons travel faster.
- Collision dynamics: After interaction, solitons recover their shape with only a phase shift.

These properties make solitons excellent test cases for numerical solvers, especially those intended to simulate nonlinear wave propagation in microstructured media.

2.5 Purpose of Analytical Solutions in This Work

Analytical solutions serve two main purposes in this thesis:

1. Initial Conditions: They provide well-defined wave profiles to initialize numerical simulations.
2. Validation Reference: They allow quantitative and qualitative comparison with numerical solutions to verify the scheme's accuracy.

In the later sections, we will compare numerical results with the analytical one- and two-soliton solutions presented here. Deviations will be analyzed in terms of amplitude error, phase shift, and shape distortion.

3 Finite Volume Scheme

3.1 Overview

The Boussinesq-type equation models wave propagation and includes both nonlinear and dispersive effects. Analytical solutions, while useful, are limited to ideal cases. Therefore, numerical methods are essential for studying general wave interactions and soliton dynamics.

The finite volume method (FVM) is well-suited for this task. It is based on integrating the governing equations over discrete control volumes and evaluating intercell fluxes. This method conserves quantities like momentum and energy and is particularly useful for hyperbolic systems (LeVeque, 1992; 2002).

In this section, we construct a finite volume scheme for the normalized Boussinesq-type equation:

$$u_{tt} - u_{xx} + \beta(u^2)_{xx} + \alpha u_{xxxx} = 0, \tag{3.1}$$

where β is the nonlinear coefficient and α is the dispersive coefficient.

Our approach follows the local equilibrium approximation and excess quantity formulation in which computational cells are treated as locally equilibrated subsystems, and cell interactions are governed by interface excess quantities derived from Riemann invariants (Berezovski, 2011).

3.2 Reformulation as a First-Order System

To discretize the Boussinesq equation with the finite volume method, it is convenient to rewrite it as a first-order system. For this purpose, we introduce an auxiliary variable w (x, t) defined by:

$$w_x = u_t, \tag{3.2}$$

Substituting this relation into the Good Boussinesq equation and integrating once with respect to x gives:

$$w_t = u_x - \beta(u^2)_x - \alpha u_{xxx}, \tag{3.3}$$

Therefore, the system takes the form:

$$u_t = w_x, \tag{3.4}$$

$$w_t = u_x - \beta(u^2)_x - \alpha u_{xxx}. \tag{3.5}$$

3.3 Local Equilibrium Approximation

Following the thermodynamic interpretation of Berezovski (2011), each computational cell is treated as a local equilibrium system. The field variables are decomposed as:

$$u = \bar{u} + U, \;\; w = \bar{w} + W, \tag{3.6}$$

where:

- $\bar{u}, \bar{w}$ are cell-averaged (local equilibrium) quantities.
- U, W are excess (non-equilibrium) quantities representing deviations at cell interfaces.

3.4 Finite Volume Method

We apply the finite volume method by integrating the system over a computational cell $C_n = [x_n, x_{n+1}]$ of width Δx.

Integration of $u_t = w_x$:

Integrating over cell n:

$$\frac{d}{dt}\int_{x_n}^{x_{n+1}} u dx = \int_{x_n}^{x_{n+1}} w_x dx\,, \tag{3.7}$$

$$\Delta x \frac{\partial \bar{u}_n}{\partial t} = w_{n+\frac{1}{2}} - w_{n-\frac{1}{2}}. \tag{3.8}$$

The flux difference is approximated using excess quantities W_n^+(right boundary) and W_n^- (left boundary) relative to w_n:

$$\Delta x \frac{\partial \bar{u}_n}{\partial t} = (\bar{w}_n + W_n^+) - (\bar{w}_n + W_n^-) = (W_n^+ - W_n^-), \tag{3.9}$$

$$\frac{\partial \bar{u}_n}{\partial t} = \frac{1}{\Delta x}(W_n^+ - W_n^-). \tag{3.10}$$

Integration of $w_t = (u - \beta u^2)_x - \alpha u_{xxx}$:

Integrating over cell n:

$$\Delta x \frac{\partial \bar{w}_n}{\partial t} = \int_{x_n}^{x_{n+1}} (u - \beta u^2)_x \, dx - \alpha \int_{x_n}^{x_{n+1}} u_{xxx} dx\,, \tag{3.11}$$

$$\Delta x \frac{\partial \bar{w}_n}{\partial t} = [u - \beta u^2]_{x_n}^{x_{n+1}} - \alpha [u_{xx}]_{x_n}^{x_{n+1}}. \tag{3.12}$$

We evaluate the contribution of each part:

1. **Non-dispersive Flux Term:**

$$[u - \beta u^2]_{x_n}^{x_{n+1}} = F(u)|_{n+\frac{1}{2}} - F(u)|_{n-\frac{1}{2}}, \tag{3.13}$$

where $F(u) = u - \beta u^2$.

Evaluating this flux difference using the average $\bar{u}_n$ and excess quantities $U_n^{\pm}$ gives:

$$F(u)|_{n+\frac{1}{2}} - F(u)|_{n-\frac{1}{2}} = [(\bar{u}_n + U_n^+) - \beta(\bar{u}_n + U_n^+)^2] - [(\bar{u}_n + U_n^-) - \beta(\bar{u}_n + U_n^-)^2]$$

$$= U_n^+ - U_n^- - 2\beta\bar{u}_n U_n^+ + 2\beta\bar{u}_n U_n^- - \beta(U_n^+)^2 + \beta(U_n^-)^2. \tag{3.14}$$

2. Dispersive Term:

$$-\alpha[u_{xx}]_{x_n}^{x_{n+1}} = -\alpha\left(u_{xx}|_{n+\frac{1}{2}} - u_{xx}|_{n-\frac{1}{2}}\right). \tag{3.15}$$

This arises from integrating $-\alpha u_{xxx} = -\alpha(u_{xx})_x$.

Following the finite volume methodology, we approximate the flux $D = -\alpha u_{xx}$ at the cell interfaces using a standard second-order centered approximation:

$$u_{xx}|_{n+\frac{1}{2}} \approx \frac{\bar{u}_{n+2} - 2\bar{u}_{n+1} + \bar{u}_n}{(\Delta x)^2}, \tag{3.16}$$

$$u_{xx}|_{n-\frac{1}{2}} \approx \frac{\bar{u}_n - 2\bar{u}_{n-1} + \bar{u}_{n-2}}{(\Delta x)^2}. \tag{3.17}$$

Substituting these gives the contribution to $\Delta x \frac{\partial \bar{w}_n}{\partial t}$:

$$-\alpha\left(u_{xx}|_{n+\frac{1}{2}} - u_{xx}|_{n-\frac{1}{2}}\right) \approx -\alpha\left(\frac{\bar{u}_{n+2} - 2\bar{u}_{n+1} + \bar{u}_n}{(\Delta x)^2} - \frac{\bar{u}_n - 2\bar{u}_{n-1} + \bar{u}_{n-2}}{(\Delta x)^2}\right)$$

$$= -\frac{\alpha}{(\Delta x)^2}(\bar{u}_{n+2} - 2\bar{u}_{n+1} + 2\bar{u}_{n-1} - \bar{u}_{n-2}). \tag{3.18}$$

3.5 Semi-Discrete Equations:

Combining these results, the semi-discrete system for the cell averages is:

$$\frac{\partial \bar{u}_n}{\partial t} = \frac{1}{\Delta x}(W_n^+ - W_n^-), \tag{3.19}$$

$$\frac{\partial \bar{w}_n}{\partial t} = \frac{1}{\Delta x}\begin{bmatrix} U_n^+ - U_n^- - 2\beta\bar{u}_n U_n^+ + 2\beta\bar{u}_n U_n^- - \beta(U_n^+)^2 + \beta(U_n^-)^2 \\ -\frac{\alpha}{(\Delta x)^2}(\bar{u}_{n+2} - 2\bar{u}_{n+1} + 2\bar{u}_{n-1} - \bar{u}_{n-2}) \end{bmatrix}. \tag{3.20}$$

The equation (3.20) can be written as:

$$\frac{\partial \bar{w}_n}{\partial t} = \frac{1}{\Delta x}[U_n^+ - U_n^- - 2\beta \bar{u}_n U_n^+ + 2\beta \bar{u}_n U_n^- - \beta (U_n^+)^2 + \beta (U_n^-)^2] - \frac{\alpha}{(\Delta x)^3}(\bar{u}_{n+2} - 2\bar{u}_{n+1} + 2\bar{u}_{n-1} - \bar{u}_{n-2}). \quad (3.21)$$

3.6 Time Integration

The numerical scheme is integrated in time using the second-order Runge-Kutta (RK2) method, which offers improved accuracy and stability over the standard Euler method (LeVeque, 2002). At each time step, two intermediate evaluations of the right-hand side (RHS) are performed: one at the current time level and one at a midpoint estimate. The final update is computed by averaging these two RHS evaluations. This approach enhances the ability of the solver to capture nonlinear and dispersive wave interactions with better temporal resolution.

3.6.1 Fully Discrete Scheme

In implementation, we use a second-order Runge–Kutta scheme for improved accuracy.

Update for $\bar{u}_n$

$$\bar{u}_n^{k+1} = \bar{u}_n^k + \frac{\Delta t}{\Delta x}(W_n^+ - W_n^-)^k. \quad (3.22)$$

Update for $\bar{w}_n$

$$\bar{w}_n^{k+1} = \bar{w}_n^k + \frac{\Delta t}{\Delta x}[U_n^+ - U_n^- - 2\beta \bar{u}_n U_n^+ + 2\beta \bar{u}_n U_n^- - \beta (U_n^+)^2 + \beta (U_n^-)^2]^k - \Delta t \left(\frac{\alpha}{(\Delta x)^3}(\bar{u}_{n+2} - 2\bar{u}_{n+1} + 2\bar{u}_{n-1} - \bar{u}_{n-2}) \right)^k. \quad (3.23)$$

Here k denotes the time level $t_k = k\Delta t$. The superscript 'k' outside the parentheses indicates that all terms within those parentheses $\bar{u}_n, U_n^+, U_n^-$ are evaluated using values known at time level k.

Riemann invariants

For the linearized system (α = β = 0), the governing equations reduce to:

$$u_t = w_x, \qquad w_t = u_x. \quad (3.24)$$

The characteristic variables are the Riemann invariants

$$R^+ = w + u_x, \quad R^- = w - u_x, \quad (3.25)$$

These describe right- and left-propagating waves, respectively. Using this property, the interface relations become:

$$W_n^+ = U_n^+, \; W_n^- = -U_n^-. \quad (3.26)$$

This connection ensures that the fluxes are represented consistently in terms of the excess quantities.

Excess quantities at time level k

The excess quantities U_n^+ (contribution from interface $n + 1/2$) and U_n^- (contribution from interface $n - 1/2$) are calculated at time level k using the Riemann invariants based on $\bar{u}^k, \bar{w}^k$ from adjacent cells:

$$U_n^+ = \frac{1}{2}(\bar{u}_{n+1}^k - \bar{u}_n^k + \bar{w}_{n+1}^k - \bar{w}_n^k)(\text{Associated with right interface of cell n})$$

$$U_n^- = \frac{1}{2}(-\bar{u}_n^k + \bar{u}_{n-1}^k + \bar{w}_n^k - \bar{w}_{n-1}^k)(\text{Associated with left interface of cell n})$$

3.6.2 Stability Considerations

Although the explicit Euler method is easy to implement, its stability depends on the CFL (Courant–Friedrichs–Lewy) condition (Courant et al., 1928), which in our case is influenced by:

- The maximum wave speed (related to the soliton speed c).
- The nonlinear coefficient β.
- The dispersive coefficient α.
- The spatial step size Δx.

In practice, the time step Δt is chosen small enough such that:

$$\Delta t \leq C \cdot \frac{\Delta x}{\max|c_{\text{eff}}|}, \tag{3.27}$$

where $C < 1$ is a safety factor and c_{eff} is an effective wave speed based on the analytical soliton.

For simulations involving high-order dispersion and nonlinear steepening, smaller values of Δt are often necessary to prevent numerical instabilities.

3.6.3 Implementation Notes

- Initial Conditions: Values of $\bar{u}_n^0$ and $\bar{w}_n^0$ are set using the analytical one- or two-soliton solution.
- Ghost Cells: The stencil for the dispersive term requires data at $n \pm 2$. Thus, ghost cells (padding cells) are used at the boundaries to ensure correct evaluations.
- Filtering (optional): In long-time simulations, applying a Savitzky–Golay filter (Savitzky & Golay, 1964) or other smoothing filter to $\bar{u}_n$ or $\bar{w}_n$ can help reduce spurious oscillations introduced by dispersive effects.

3.6.4 Summary of Algorithm Steps

1. **Initialize:**
   - $\bar{u}_n^0 = u(x_n, 0)$
   - $\bar{w}_n^0 =$ value defined consistently with the analytical initial condition.
     - For a single soliton moving to the right with velocity c: $\bar{w}_n^0 = -c \cdot u(x_n, 0)$.
     - For two solitons moving in opposite directions: $\bar{w}_n^0 = -c \cdot u_1(x_n, 0) + c \cdot u_2(x_n, 0)$.
2. **At each time step k:**
   - Apply boundary conditions (ghost cells)
   - Compute excess quantities U_n^+, U_n^-
   - Update $\bar{u}_n^{k+1}$ using the flux difference
   - Update $\bar{w}_n^{k+1}$ using the full RHS (linear, nonlinear, dispersive terms)
3. **Repeat until final time**

3.6.5 Filtering

To reduce numerical noise—especially from steep gradients and dispersive interactions—a Savitzky-Golay filter (Savitzky & Golay, 1964) is applied after each time step to both u and w. This post-processing step preserves the overall shape of the solution while suppressing spurious oscillations introduced by discretization.

4 Initial Conditions

To simulate solitonic wave propagation in microstructured solids, the numerical scheme must be initialized with suitable wave profiles that reflect the physical properties of the Boussinesq-type equation. This section presents the analytical soliton solution used to define initial conditions for both single- and two-soliton configurations. These profiles serve as a benchmark for validating the finite volume scheme and observing nonlinear interactions such as collision and separation.

4.1 Single-Soliton Initial Condition

We begin with the analytical single-soliton solution of the Good Boussinesq-type equation, which provides a benchmark for validating the numerical scheme (Bona et al., 2002; Drazin, 1989). The solitary-wave form is:

$$u(x,t) = A \cdot \operatorname{sech}^2\big(\kappa(x - ct - x_0)\big), \tag{4.1}$$

where:

- $u(x,t)$ is the displacement field.
- A is the amplitude of the wave.
- k is the inverse width parameter.
- c is the soliton speed.
- x_0 is the initial center of the pulse.

The parameters A and k are related to the nonlinear and dispersive coefficients β and α via:

$$A = \frac{3(c^2-1)}{2\beta},$$
$$\kappa = \sqrt{\frac{(c^2-1)}{4\alpha}}. \tag{4.2}$$

These expressions ensure that the initial profile satisfies the governing equation under steady-state propagation. The parameter κ directly controls the spatial width of the soliton: larger κ values produce narrower and taller pulses, whereas smaller values yield broader and flatter profiles.

In our simulation, we set the initial time t = 0, and the initial displacement is defined as:

$$u(x,t) = A \cdot \operatorname{sech}^2\big(\kappa(x - x_0)\big), \tag{4.3}$$

where x_0 is chosen to center the pulse within the computational domain to avoid interaction with boundaries. Typically, $x_0 = L/2$ for a domain of length L.

The corresponding auxiliary variable $w(x,t)$, associated with momentum, can be determined by:

$$w(x,0) = -c\frac{\partial u}{\partial x}(x,0). \tag{4.4}$$

Evaluating this derivative yields:

$$w(x,0) = 2Ac\kappa \cdot \operatorname{sech}^2[\kappa(x - x_0)] \cdot \tanh[\kappa(x - x_0)]\,. \tag{4.5}$$

This formulation ensures that the initial wave is not only shaped correctly but also travels in the positive x-direction due to the positive momentum imparted by $w(x,0)$. The corresponding analytical profiles of $u(x,0)$ and $w(x,0)$ are displayed in Figure **4.1**, which illustrates the initial soliton shape and its associated momentum distribution derived from the analytical solution of the Boussinesq-type equation (Bona et al., 2002; Sjölander, 2021).

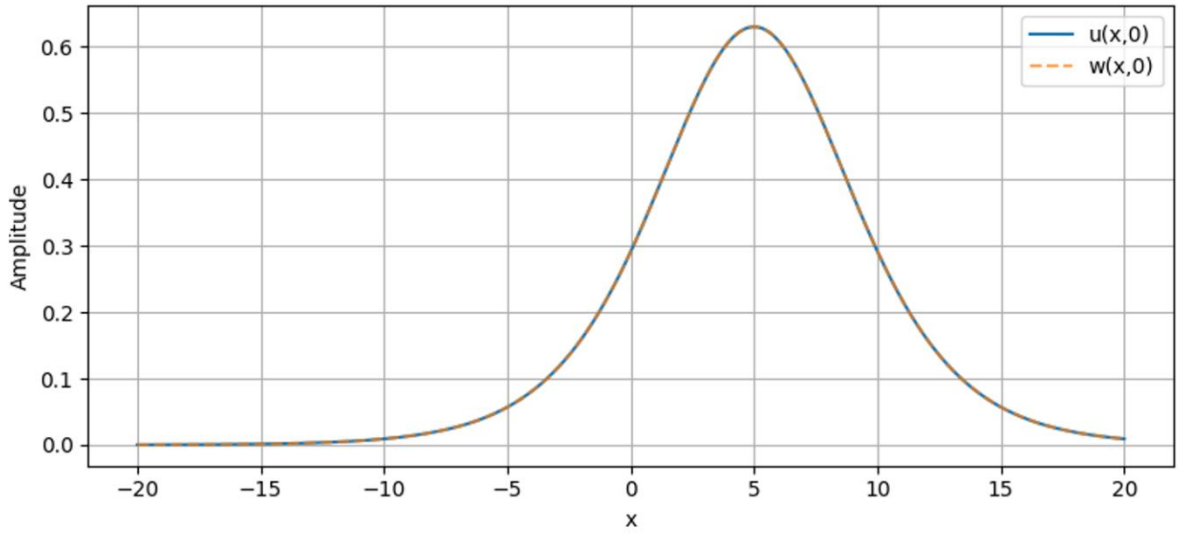

Figure 4.1: Initial displacement u(x,0) and corresponding velocity field w(x,0) for a single soliton centered at $x_0 = 5$. The fields are computed from the analytical solution of the normalized Boussinesq-type equation

4.2 Initial Condition with Two Solitons

To study nonlinear wave interaction, the initial condition is extended to include two counter-propagating solitons constructed from the analytical single-soliton profiles described in Section 4.1 (Bona et al., 2002; Sjölander, 2021). The total displacement field is constructed by superposing two single solitons centered at symmetric positions:

$$u(x,t) = A \cdot \operatorname{sech}^2\big(\kappa(x - x_0)\big) + A \cdot \operatorname{sech}^2\big(\kappa(x + x_0)\big). \tag{4.6}$$

In this setup, the first soliton is centered at $+x_0$ and propagates to the left, while the second is centered at $-x_0$ and propagates to the right. The symmetry of the configuration allows us to observe collision and separation dynamics without interference from boundaries, provided the domain is sufficiently large.

The initial momentum field $w(x,0)$ is derived by taking the time derivative of the analytical solution:

$$w(x,0) = -c \cdot \frac{\partial u_1}{\partial x}(x,0) + c \cdot \frac{\partial u_2}{\partial x}(x,0). \tag{4.7}$$

Since the total displacement is a sum of two solitons, the resulting momentum becomes:

$$w(x,0) = -2Ac\kappa \cdot \operatorname{sech}^2[\kappa(x - x_0)] \cdot \tanh[\kappa(x - x_0)] \\ +2Ac\kappa \cdot \operatorname{sech}^2[\kappa(x + x_0)] \cdot \tanh[\kappa(x + x_0)]\,. \tag{4.8}$$

This ensures that one soliton is initialized with positive momentum (moving left to right) and the other with negative momentum (moving right to left), both starting symmetrically about the origin.

The resulting analytical profiles of $u(x,0)$ and $w(x,0)$ are presented in Figure **4.2**, which visualizes the symmetric two-soliton setup used throughout the numerical experiments.

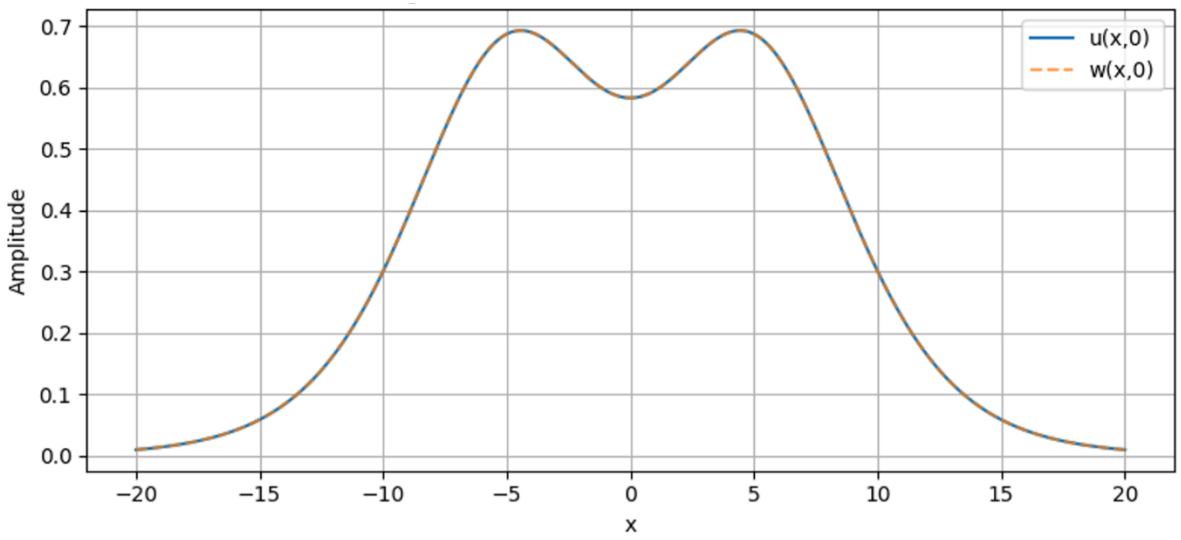

Figure 4.2: Initial displacement $u(x,0)$ and velocity field $w(x,0)$ for a two-soliton configuration.

The profile shows two identical solitons positioned symmetrically at $\pm x_0$, propagating toward each other with opposite velocities based on the analytical expression.

4.3 Effect of Soliton Width (κ)

It is important to note that the soliton width is inversely related to the parameter κ. For larger values of κ, the solitons become narrower and steeper, which can cause numerical difficulties if not adequately resolved by the spatial grid. Conversely, smaller values of κ result in broader solitons, which are easier to resolve but slower-moving.

In practice, choosing moderate values of α and c leads to manageable values of κ and well-resolved soliton shapes within a fixed grid resolution. Figure **4.3** compares analytical profiles for different κ values, highlighting how increased dispersion (larger α) broadens the soliton, whereas stronger nonlinearity (larger β) sharpens it. These analytical relations guide the parameter choices for subsequent numerical tests.

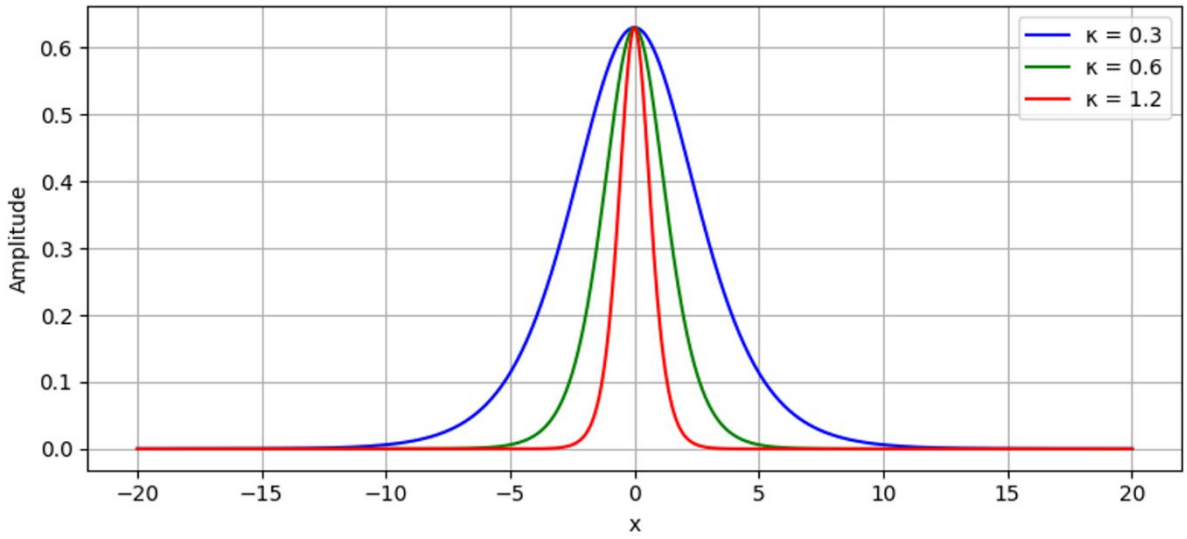

Figure 4.3: Comparison of soliton profiles for different values of the inverse width parameter κ.

Increasing κ results in sharper, narrower solitons, illustrating the sensitivity of the soliton shape to dispersion and wave speed parameters.

4.4 Spatial Domain and Grid Resolution

To ensure the accurate resolution of solitonic structures and to prevent artificial reflections from boundary conditions, specific choices must be made regarding the spatial domain and grid resolution.

The computational domain is defined over a symmetric interval $x \in [-L, L]$, where L is chosen such that the soliton(s) remain well-separated from the boundaries throughout the simulation time. For all numerical experiments in this thesis, we typically set L = 20 or larger depending on the soliton width and speed.

The spatial resolution is governed by the grid spacing $\Delta x = \frac{2L}{N}$, where N is the number of grid cells. To properly resolve the soliton shape, the following guideline is applied:

$$\kappa \gg \Delta x^{-1}.$$

This ensures that each soliton spans at least 20–30 spatial points, preventing numerical aliasing and capturing fine-scale features such as tails and dispersion effects.

Additionally, the total simulation time is chosen such that the solitons do not reach the boundaries, avoiding spurious reflections. When necessary, absorbing (non-reflective) boundary conditions are applied or the time integration is stopped prior to any boundary interaction.

These considerations ensure numerical stability, minimize truncation errors, and maintain physical accuracy in the comparison between numerical and analytical solutions.

5 Comparison of Numerical and Analytical Solutions

Parameter Set:

Table 1: Parameters used in the numerical simulations of the Boussinesq-type equation.

Symbol	Value / Description
α	1.5
β	0.5
c	1.10
A	0.63
κ	0.187 ($width \approx 5.34$)
Δx	0.5
Δt	0.0167
L	120
T	10
x_{01}	48
x_{02}	72
t_{meet}	≈ 10

For the numerical experiments, two initial configurations were considered: (i) separated solitons with centres $x_{01} = 36, x_{02} = 84$, which do not collide within $T = 10$, and (ii) interacting solitons with centers $x_{01} = 48, x_{02} = 72$, resulting in a collision at approximately $t \approx 10$. These values were chosen to ensure a balance between nonlinearity and dispersion while restricting simulations to about two–three soliton widths.

5.1 Overview

This chapter validates the finite volume scheme introduced in Chapter 3 by comparing its predictions with known analytical solutions of the good Boussinesq equation. Both single- and two-soliton problems are studied in order to test the scheme's ability to capture propagation, interaction, and recovery of solitons. In addition to qualitative comparisons of numerical and analytical profiles, a three-dimensional representation is provided to visualize the interaction, and quantitative accuracy is assessed using the L^2 error norm.

5.2 Single Soliton Propagation

As a first validation, a single right-moving soliton was simulated with the parameters listed in the parameter set. The analytical soliton solution has amplitude A = 0.63 and width $\kappa^{-1} \approx 5.34$. The

initial condition was centered at x_0 = 0.35 L, with $w(x,0) = -cu(x,0)$, ensuring consistency with the definition $u_t = w_x$.

Figure **5.1** shows the surface plot of numerical solution $u(x,t)$ over the simulation window $T = 10$. The soliton crest follows a clear diagonal trajectory, corresponding to the constant soliton velocity $c = 1.10$. The soliton maintains both shape and amplitude without noticeable distortion, indicating that the scheme successfully balances the nonlinear and dispersive Boussinesq-type equation.

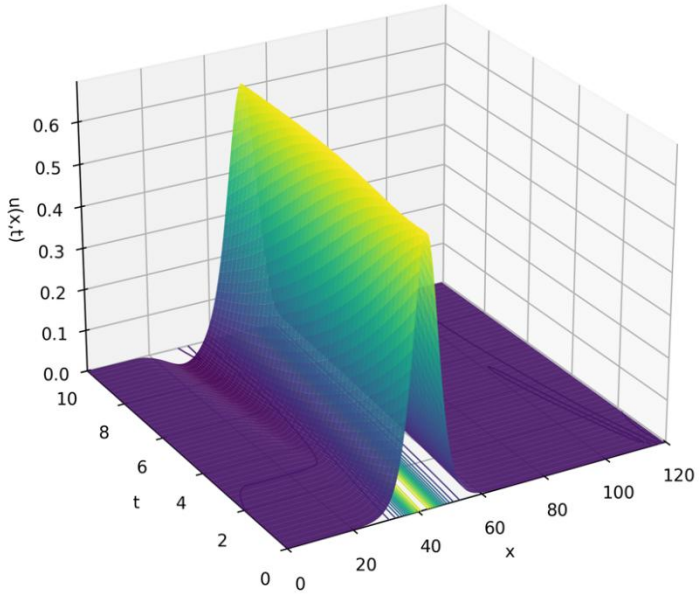

Figure 5.1: Numerical propagation of a single soliton using the finite volume scheme.

Parameters: α=1.5, β=0.5, c=1.10, A=0.63, κ=0.187 (width ≈5.34), Δx=0.5, Δt=0.0167, L=120, T=10 The soliton crest follows a diagonal trajectory at constant velocity, preserving amplitude and shape without distortion.

To further clarify the soliton motion, Figure **5.2** presents the contour map of $u(x,t)$.

The bright ridge represents the crest of the soliton, while the dashed line indicates the analytical trajectory of the soliton center, derived from the argument of the analytical solution

$$u(x,t) = A \cdot \operatorname{sech}^2\big(\kappa(x - ct - x_0)\big), \tag{5.1}$$

which implies that the peak moves at a constant speed c.

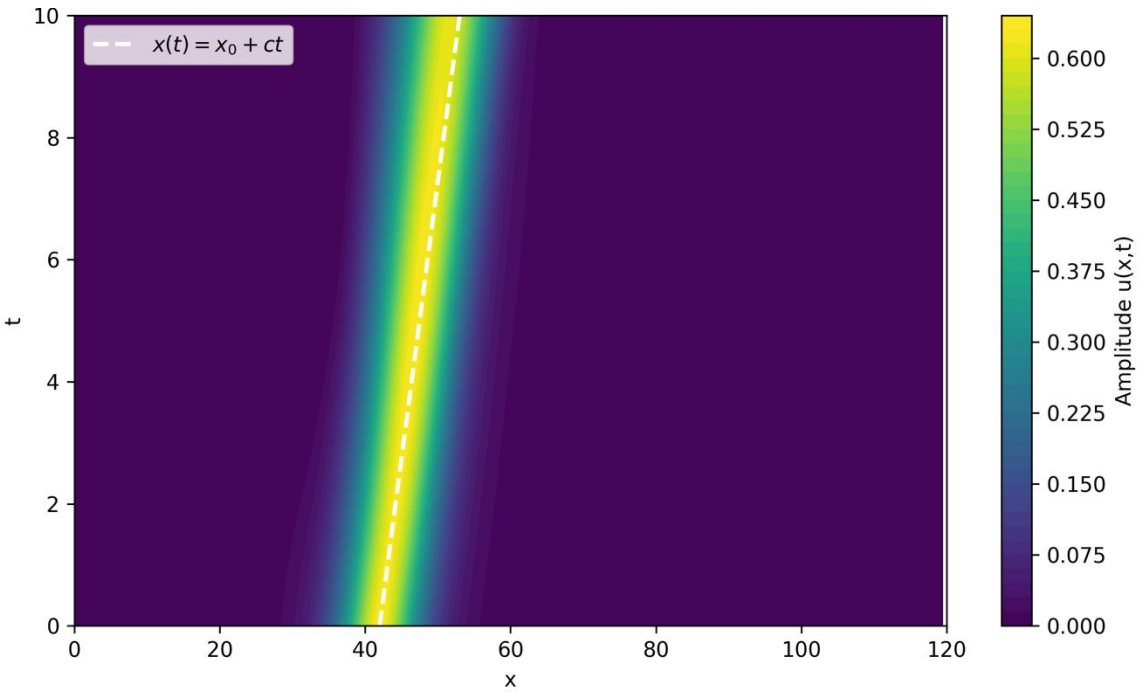

Figure 5.2: Contour map of the numerical single-soliton solution $u(x,t)$.

Parameters as in Figure 5.1.

Together, the surface and contour plots verify that the numerical implementation provides a stable and highly accurate representation of single-soliton dynamics.

5.3 Two Solitons Propagation Comparison at Selected Times

To further challenge the scheme, the head-on interaction of two solitons was studied. The initial positions were chosen as $x_{01} = 36$ and $x_{02} = 84$. With this configuration, the solitons approach one another but do not collide within the simulated time $T = 10$. This test isolates the propagation dynamics and validates numerical stability over long distances without the complexity of interaction.

Figure **5.3** presents the numerical and analytical solutions at selected times $(t = 0,3,5,8)$. These time instants were chosen to illustrate the pre-interaction phase: at $t = 0$ the solitons are well separated; at $t = 3$ and $t = 5$ they approach each other; and at $t = 8$ they are close but have not yet overlapped. When the solitons are far apart $(t = 0,3)$, the agreement is nearly exact. As the waves approach $(t = 5, 8)$, minor discrepancies appear near the crests, but the solitons retain their speed and shape. The shaded error regions remain small, demonstrating that the scheme accurately tracks soliton propagation even as the waves converge.

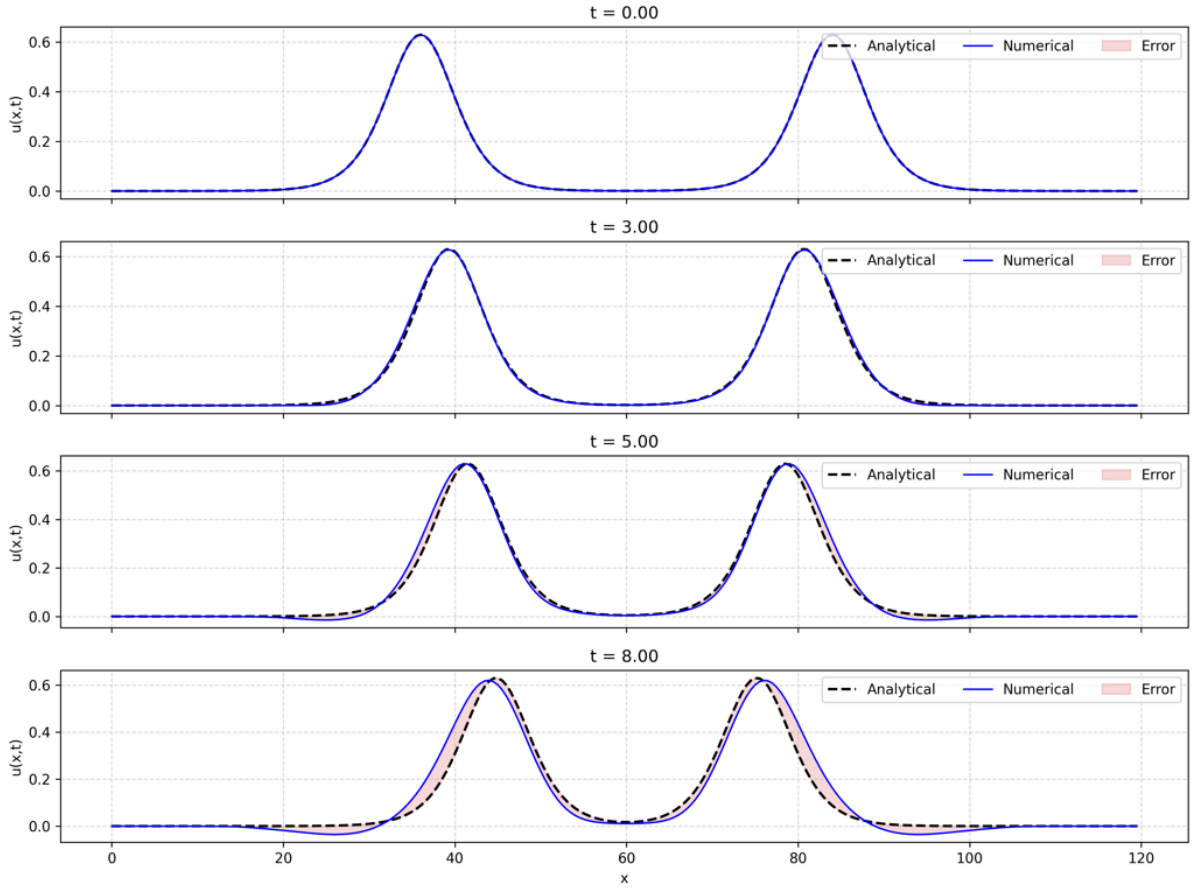

Figure 5.3: Two-soliton propagation without collision (pre-collision).

Numerical and analytical profiles compared at t=0, 3, 5, and 8. Parameters: α=1.5, β=0.5, c=1.10, A=0.63, κ=0.187, Δx=0.5, Δt=0.0167, L=120, T=10; centers x_{01}=36, x_{02}=84.

5.4 Two Solitons Interaction (Collision)

To evaluate the scheme under nonlinear interaction, the solitons were initialized closer, at $x_{01} = 48$ and $x_{02} = 72$. In this configuration, the solitons approach each other and collide at approximately t = 10.

Figure **5.4** shows the numerical and analytical solutions at two representative times: the initial state $(t = 0)$ and during collision $(t = 10)$. At $t = 0$, the numerical and analytical profiles coincide almost perfectly, confirming that the initial condition is well captured. During the collision, the numerical scheme slightly underestimates the crest height compared to the analytical solution. Nevertheless, the overall timing and structure of the interaction are accurately preserved.

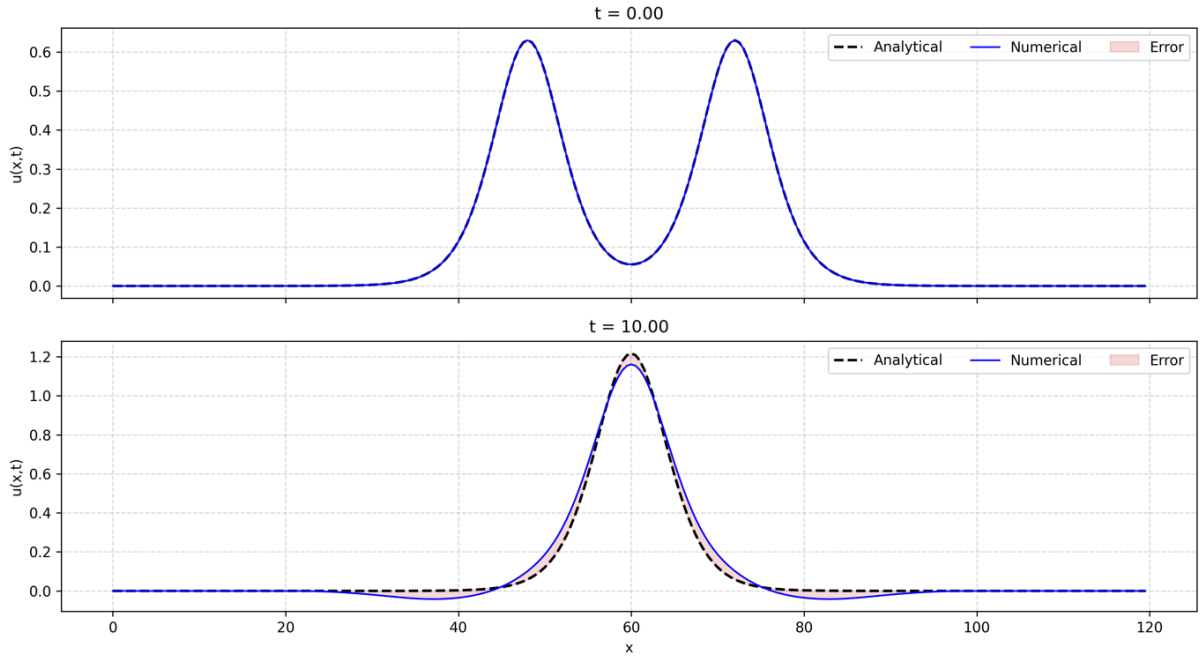

Figure 5.4: Two-soliton interaction with collision.

Numerical and analytical profiles compared at $t = 0$, and during collision $(t = 10)$. Parameters as in separated case, except centers $x_{01} = 48, x_{02} = 72$.

5.5 Surface Visualization

To illustrate the full spatiotemporal evolution of the interaction, we render the numerical solution $u(x, t)$as a surface plot (Figure **5.5**). Two diagonal ridges are visible: they represent the trajectories of the right-moving and left-moving solitons. As the waves approach, a localized, transient increase in amplitude is observed near the center of the domain. The surface view is useful for seeing the overall geometry of the interaction and the absence of spurious oscillations away from the soliton cores.

Because the perspective and shading of a 3D surface can mask fine timing and trajectory details, we also provide a **contour map** of $u(x, t)$on the (x, t)-plane (Figure **5.6**). In this representation the soliton crests appear as bright bands whose separation decreases during approach and increases after interaction. The contour map complements the surface plot view by making the propagation paths and the near-collision region clearly visible without depending on viewpoint.

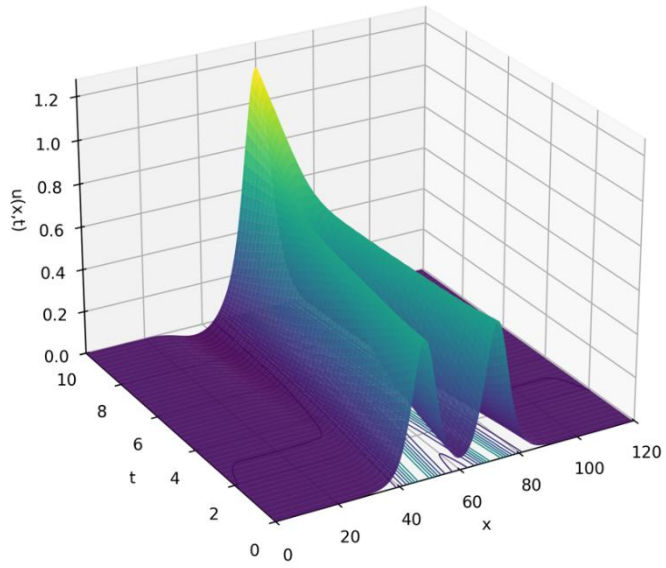

Figure 5.5: The surface plot view of two-soliton interaction (good Boussinesq).

Diagonal ridges represent soliton trajectories; a transient amplitude increase is observed during interaction before recovery. Parameters: α=1.5, β=0.5, c=1.10, A=0.63, κ=0.187, Δx=0.5, Δt=0.0167, L=120, T=10.

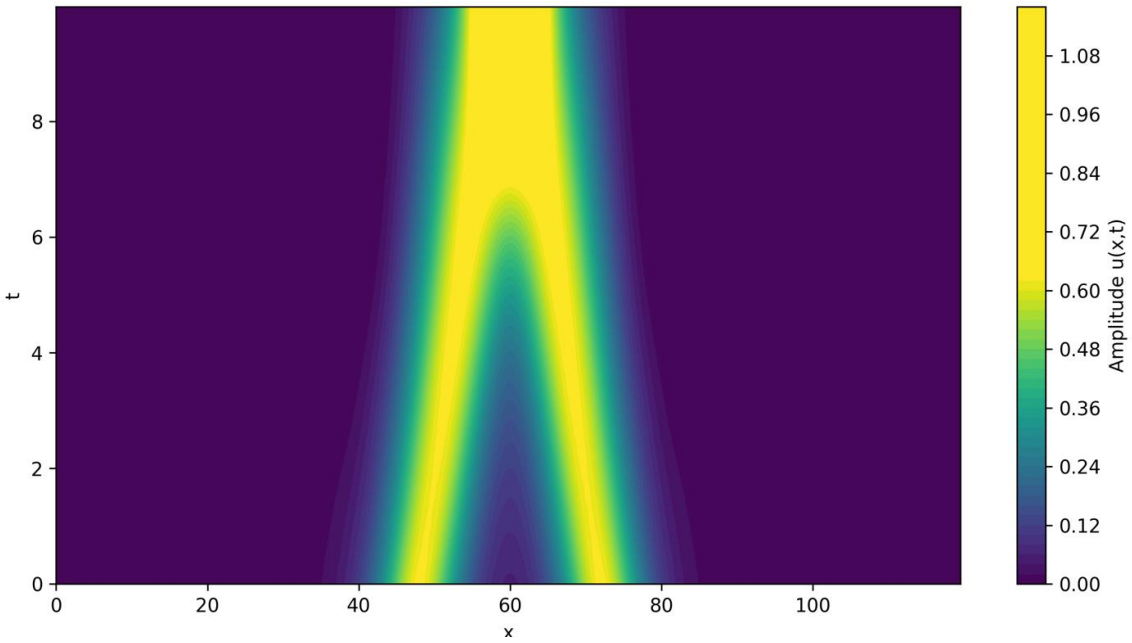

Figure 5.6: Contour map of $u(x,t)$ for the two-soliton case.

The bands corresponding to the two crests approach, overlap locally, and then separate, providing a clear 2D view of the interaction that complements Figure 5.5.

5.6 L^2 Error Norm Analysis

To quantify the accuracy of the numerical method, the L^2 error norm between the numerical and analytical solutions was computed at each time step using:

$$L^2(t) = \sqrt{\int \left(u_{\text{num}}(x,t) - u_{\text{ana}}(x,t)\right)^2 dx}. \tag{5.2}$$

Figure **5.7** shows the error evolution over time. The error remains negligible during the early stages of propagation, rises during the collision, and stabilizes afterwards. This behaviour reflects the increased numerical challenge at the point of constructive overlap but confirms that the scheme maintains stability and bounded error throughout.

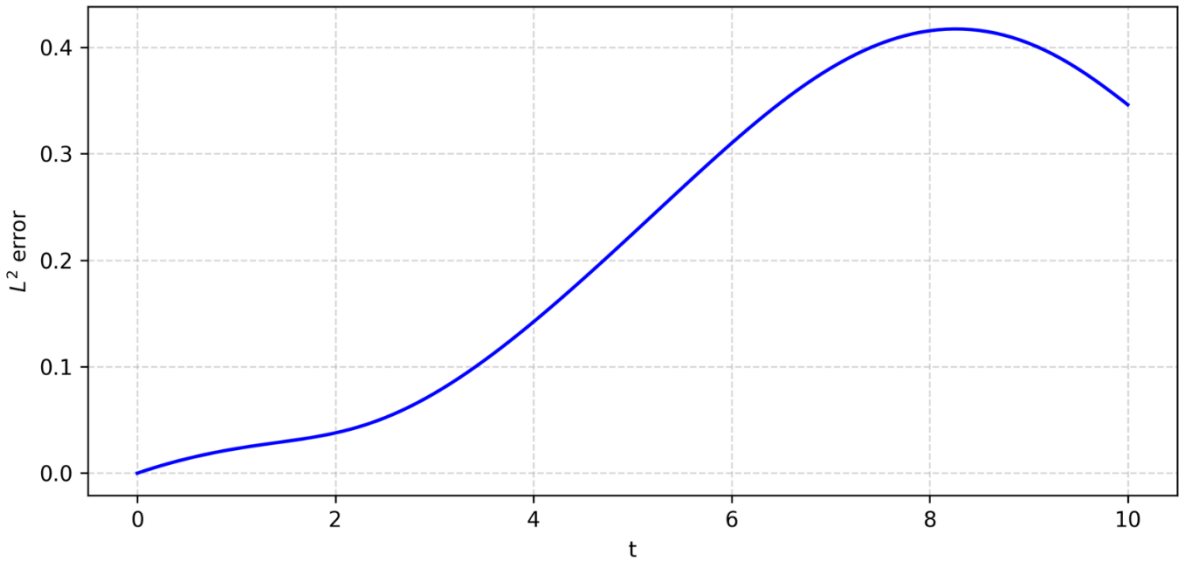

Figure 5.7: L^2 error vs time for two-soliton interaction. Error rises during collision but remains small overall, stabilizing after separation.

5.7 Discussion

The combined tests demonstrate that the finite volume scheme accurately reproduces soliton behaviour in the Boussinesq equation. The single soliton case validated the method's ability to preserve amplitude and trajectory. The two-soliton propagation confirmed stability and agreement with analytical profiles across multiple soliton widths. The collision test showed that the scheme captures constructive overlap with only minor amplitude underestimation. Finally, the L^2 error analysis provided quantitative confirmation of accuracy and robustness.

Together, these results demonstrate that the scheme successfully balances nonlinearity and dispersion and can describe both soliton propagation and soliton interaction with high fidelity.

6 Extension of the Boussinesq Equation with Internal Variables

6.1 Theoretical Background

Wave propagation in solids with microstructure cannot be fully described by the classical Boussinesq equation, which accounts only for macroscopic strain and its gradients. To incorporate internal degrees of freedom associated with the microstructure, the framework of internal variables is adopted (Berezovski et al., 2013).

Before introducing this generalized formulation, the classical free-energy density leading to the standard Boussinesq equation is briefly reviewed.

Free energy

Free energy per unit volume corresponding to the Boussinesq equation can be expressed as:

$$\psi = \frac{\rho c^2}{2} u_x^2 - a(u^2)_x u_x - D u_{xxx} u_x, \tag{6.1}$$

where

- ρ is the matter density.
- c is the sound velocity.
- a is the coefficient of quadratic nonlinearity.
- D is the dispersive material constant.

The first term represents linear elastic energy, the second introduces weak nonlinearity, and the third accounts for dispersion associated with strain gradients.

From the balance of momentum

$$\frac{\partial}{\partial t}(\rho v) = \frac{\partial \sigma}{\partial x}, \tag{6.2}$$

together with the stress calculation

$$\sigma = \frac{\partial \psi}{\partial u_x} = \rho c^2 u_x - a(u^2)_x - D u_{xxx}, \tag{6.3}$$

the governing equation becomes

$$(\rho u)_{tt} - \rho c^2 u_{xx} + a(u^2)_{xx} + D u_{xxxx} = 0. \tag{6.4}$$

Dividing by ρ and normalizing leads to the classical Boussinesq-type equation

$$u_{tt} - c^2 u_{xx} + \frac{a}{\rho}(u^2)_{xx} + \frac{D}{\rho} u_{xxxx} = 0. \tag{6.5}$$

This form captures the balance between nonlinearity and dispersion that supports soliton solutions.

Extended free energy (with internal variable)

To capture the influence of microstructure, the free energy density is extended to depend not only on the strain u_x but also on an additional internal variable φ:

$$\psi = \frac{\rho c^2}{2} u_x^2 - a(u^2)_x u_x - D u_{xxx} u_x + B \varphi_x u_x + \frac{1}{2} C \varphi^2, \tag{6.6}$$

where

- ρ is the mass density.
- c is the linear wave speed.
- a is the coefficient of quadratic nonlinearity.
- D is the dispersive material constant.
- B, C describe the coupling and stiffness of the internal variable.

Macrostress and Equation of Motion

The corresponding macrostress is obtained from the derivative of the free energy with respect to the strain component u_x:

$$\sigma = \frac{\partial \psi}{\partial u_x} = \rho c^2 u_x - a(u^2)_x - D u_{xxx} + B \varphi_x. \tag{6.7}$$

The balance of linear momentum can then be written as:

$$\rho u_{tt} = \rho c^2 u_{xx} - a(u^2)_{xx} - D u_{xxxx} + B \varphi_{xx}. \tag{6.8}$$

For a non-dissipative microstructured solid (Berezovski, 2017), the internal variable obeys a simple proportionality law between the strain curvature and the microstructural response

$$B u_{xx} - C \varphi = 0, \tag{6.9}$$

which yields the relation

$$\varphi = \frac{B}{C} u_{xx}. \tag{6.10}$$

This relation implies that the internal variable is directly proportional to strain gradient.

Final governing equation

By substituting Eq. (6.10) into Eq. (6.8), one obtains a single governing equation for the displacement field $u(x, t)$:

$$\rho u_{tt} = \rho c^2 u_{xx} - a(u^2)_{xx} - D u_{xxxx} + \frac{B^2}{C} u_{xxxx}. \tag{6.11}$$

Dividing by ρ gives the normalized form

$$u_{tt} - c^2 u_{xx} + \frac{a}{\rho}(u^2)_{xx} + \left(\frac{D}{\rho} - \frac{B^2}{\rho C}\right) u_{xxxx} = 0, \tag{6.12}$$

which represents the Boussinesq-type equation with an internal variable. The last term modifies the effective dispersive coefficient and thereby alters the soliton shape.

When $B = 0$, the equation reduces to the classical Boussinesq form, while for finite B and C, the influence of the internal variable increases the effective dispersion, slightly narrowing and localizing the soliton compared to the classical case.

Connection to the classical Boussinesq form

Comparing with the classical Boussinesq equation used in Sections 2–5,

$$u_{tt} - c^2 u_{xx} + \frac{a}{\rho}(u^2)_{xx} + \alpha_{\text{eff}} u_{xxxx} = 0, \tag{6.13}$$

we see that the presence of the internal variable modifies only the dispersive term. The effective dispersion coefficient (Bona et al., 2002; Berezovski & Engelbrecht, 2010) is

$$\alpha_{\text{eff}} = \left(\frac{D}{\rho} - \frac{B^2}{\rho C}\right), \tag{6.14}$$

which replaces α in the classical model. Depending on the values of B and C, the microstructural effect may either increase or decrease the strength of dispersion.

6.2 Modification to the Numerical Scheme

The finite volume method developed in Section 3 remains applicable for the Boussinesq equation with internal variables. The structure of the system, consisting of nonlinear and dispersive terms, is preserved. The only modification is the change in the dispersion coefficient from its classical value α to the effective one α_{eff}.

Semi-discrete scheme

For the classical case, the semi-discrete form of the governing equations was written as

$$\frac{\partial \bar{u}_n}{\partial t} = \frac{1}{\Delta x}(W_n^+ - W_n^-), \tag{6.15}$$

$$\frac{\partial \bar{w}_n}{\partial t} = \frac{1}{\Delta x}\begin{bmatrix} U_n^+ - U_n^- - 2\beta \bar{u}_n U_n^+ + 2\beta \bar{u}_n U_n^- - \beta (U_n^+)^2 + \beta (U_n^-)^2 \\ -\dfrac{\alpha}{(\Delta x)^2}(\bar{u}_{n+2} - 2\bar{u}_{n+1} + 2\bar{u}_{n-1} - \bar{u}_{n-2}) \end{bmatrix}. \tag{6.16}$$

In the presence of internal variables, the scheme retains its form, but the dispersive term is modified by replacing α with α_{eff}:

$$\alpha_{\text{eff}} = \left(\frac{D}{\rho} - \frac{B^2}{\rho C}\right). \tag{6.17}$$

Thus, the dispersive contribution becomes:

$$\frac{\partial \overline{w}_n}{\partial t} = \frac{1}{\Delta x}\begin{bmatrix} U_n^+ - U_n^- - 2\beta\bar{u}_n U_n^+ + 2\beta\bar{u}_n U_n^- - \beta(U_n^+)^2 + \beta(U_n^-)^2 \\ -\frac{\alpha_{\text{eff}}}{(\Delta x)^2}(\bar{u}_{n+2} - 2\bar{u}_{n+1} + 2\bar{u}_{n-1} - \bar{u}_{n-2}) \end{bmatrix}. \tag{6.18}$$

Fully discrete scheme

In the time discretization, no changes are required. The same explicit Runge–Kutta method as described in Section 3.6.2 can be applied, subject to the same CFL-type stability (LeVeque, 2002).

Implementation in the code

From a computational point of view, incorporating microstructural effects into the finite volume solver requires only a minor modification in the dispersive term. The constant dispersion coefficient used in the classical formulation is replaced by the effective dispersive coefficient α_{eff}, derived in Section 6.1.

This modification ensures that the influence of the coupling between the internal variable and the strain curvature is correctly represented in the numerical model. All other components of the solver—such as the computation of nonlinear fluxes, the temporal integration scheme, and the filtering strategy (Savitzky & Golay, 1964)—remain unchanged.

6.3 Numerical Experiments

To demonstrate the influence of internal variables on wave propagation, unless stated otherwise, all tests use the same spatial and temporal discretization as in Section 5, but with the dispersive coefficient replaced by

$$\alpha_{\text{eff}} = \frac{D}{\rho} - \frac{B^2}{\rho C}. \tag{6.19}$$

The finite volume scheme and time-stepping algorithm are unchanged, ensuring that any differences in the results are entirely due to the microstructural contribution. Two sets of microstructural parameters were considered in order to illustrate the limiting effects of the coupling strength.

For both cases the material density was kept constant, $\rho = 1.0$, and the classical nonlinearity and soliton velocity were the same as before, $\beta = 0.5$ and $c = 1.10$. The parameters B, C and D were adjusted to obtain two representative effective dispersion coefficients:

$$\text{Case I: } D = 1.5, B = 1.0, C = 3.0 \;\Rightarrow\; \alpha_{\text{eff}} = 0.5,$$

$$\text{Case II: } D = 1.5, B = 2.0, C = 1.0 \;\Rightarrow\; \alpha_{\text{eff}} = 3.0.$$

These two configurations represent opposite microstructural responses. The smaller α_{eff} corresponds to stronger internal coupling and reduced dispersion, producing a more localized soliton, whereas the larger α_{eff} reflects weaker coupling and enhanced dispersion that broadens the wave profile.

The soliton amplitude and inverse width for each case are determined from

$$A_{\text{sol}} = \frac{3(c^2 - 1)}{2\beta}, \tag{6.20}$$

and

$$\kappa = \sqrt{\frac{c^2 - 1}{4\alpha_{\text{eff}}}}. \tag{6.21}$$

The time step satisfies a CFL restriction combining advection and dispersion (cf. Section 3.6.2), now with α_{eff} in the dispersive bound.

6.3.1 Effect of Microstructure on Soliton Propagation

To illustrate the effect of microstructural coupling on soliton behaviour, the numerical solution of a single right-moving soliton was simulated for the three cases introduced above:

(i) The classical Boussinesq equation without internal variables ($B = 0, \alpha = 1.5$).
(ii) Case I with microstructural parameters $D = 1.5, B = 1.0, C = 3.0$, giving $\alpha_{\text{eff}} = 0.5$.
(iii) Case II with $D = 1.5, B = 2.0, C = 1.0$, giving $\alpha_{\text{eff}} = 3.0$.

All simulations used the same spatial and temporal discretization as in Section 5, ensuring that α_{eff} is the only parameter that changes.

The soliton profiles were examined at time $t_0 = 5$, corresponding to steady propagation without boundary interaction.

Figure **6.1** shows the resulting soliton shapes for the three cases. For $\alpha_{\text{eff}} = 0.5$ (Case I), the soliton becomes slightly narrower and more localized, indicating reduced dispersion and stronger confinement of wave energy.

In contrast, for $\alpha_{\text{eff}} = 3.0$ (Case II), the soliton broadens noticeably, reflecting the dominance of dispersive effects due to weaker microstructural coupling.

The classical case $\alpha = 1.5$ lies between these two extremes.

Despite these differences in width, the soliton amplitude and propagation velocity remain nearly constant for all three cases, confirming that the internal variable primarily alters the dispersive character of the medium while preserving the nonlinear amplitude–velocity balance.

This demonstrates that the microstructural model provides a physically consistent mechanism for dispersion tuning through internal coupling strength.

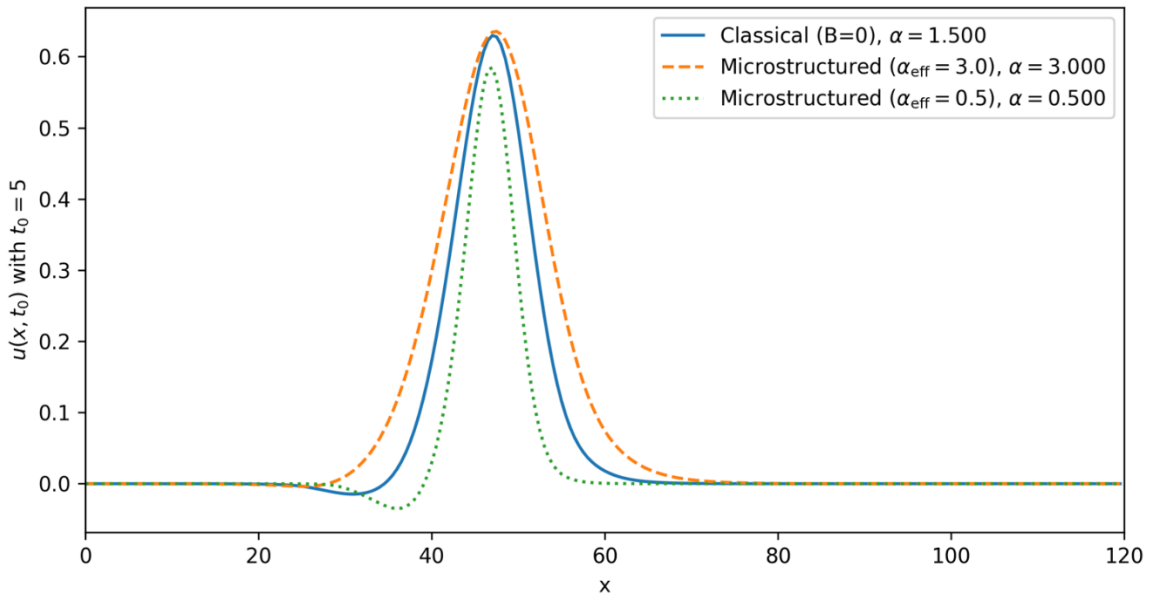

Figure 6.1: Soliton profiles with and without internal variables.

B=0 (classical Boussinesq equation, α=1.50) and B≠0 (microstructured case, $\alpha_{eff} = 3.0$ and $\alpha_{eff} = 0.5$) at t_0=5.

6.3.2 Discussion

The numerical experiments incorporating internal variables highlight the sensitivity of soliton dynamics to microstructural effects. The introduction of the effective dispersion coefficient α_{eff} modifies the soliton width and phase behaviour while preserving the overall amplitude–velocity balance. These findings are consistent with earlier theoretical and numerical studies on dispersive wave propagation in microstructured solids (Engelbrecht et al., 2005; Engelbrecht et al., 2007; Engelbrecht et al., 2011).

By systematically varying α_{eff}, the present study demonstrates how microstructural coupling influences soliton localization. For $\alpha_{\text{eff}} = 0.5$ (strong coupling), the soliton becomes narrower and more localized due to the reduced dispersion, while for $\alpha_{\text{eff}} = 3.0$ (weak coupling), it broadens because of enhanced dispersive effects. The classical case $(\alpha = 1.5)$ represents an intermediate regime where nonlinearity and dispersion remain balanced. These observations align with the theoretical prediction that the internal coupling term $(-B^2/\rho C)$ in Eq. (6.19) adjusts the dispersive strength of the medium without altering its nonlinear character (Berezovski et al., 2013).

This demonstrates that the inclusion of internal variables provides a physically meaningful mechanism for representing microstructure within a continuum framework, bridging the gap between lattice-based models and macroscopic PDE formulations. The microstructural coupling effectively acts as a dispersive tuning parameter, allowing the model to capture a wider range of physical behaviours in structured materials.

From a computational perspective, the finite-volume scheme required only minimal modification —specifically, replacing the classical dispersion coefficient with the effective parameter. The method remained stable, accurate, and energy-conserving across all simulations. This confirms that the implemented numerical approach is both robust and flexible, capable of being extended to more complex dispersive systems or higher-dimensional microstructured solids.

6.4 Summary

The Boussinesq-type equation extended with internal variables successfully models dispersive effects arising from microstructure. By replacing the classical dispersion coefficient α with its effective counterpart $\alpha_{\text{eff}} = (D/\rho) - (B^2/(\rho C))$, the governing system captures the localization and phase-shift behaviour observed in structured materials.

The comparison between the classical and modified models (Figure 6.1) clearly demonstrates that microstructural coupling significantly influences soliton width and localization. For smaller values of α_{eff} (e.g. 0.5), the soliton becomes narrower and more localized, while larger values (e.g. 3.0) produce broader profiles due to increased dispersion. Despite these variations, the amplitude and propagation speed remain stable, confirming that the modification affects only the dispersive term without disturbing the nonlinear structure of the equation.

These findings provide a consistent numerical and physical foundation for analysing the interaction between microstructure and wave dynamics. The developed finite-volume approach proves robust and accurate for simulating nonlinear dispersive waves in both classical and microstructured continua, offering a reliable basis for future studies of wave localization and dispersion control in complex materials.

7 Conclusion

This thesis has presented a numerical investigation of a Boussinesq-type equation in microstructured solids using the finite volume method. The study was divided into two main parts: the development and validation of the numerical scheme for the classical equation, and the extension of the model to include internal variables representing microstructural effects.

In the first part, the classical Good Boussinesq equation was considered to establish a reliable computational framework. Simulations of single- and two-soliton propagation verified that the finite volume method accurately reproduces analytical results, maintaining the characteristic soliton properties of stable amplitude, velocity, and shape. The L^2 error analysis demonstrated smooth, bounded behaviour over time, confirming numerical stability and second-order accuracy of the discretization scheme.

In the second part, the equation was extended by introducing an internal variable framework that modifies the dispersive coefficient through the effective parameter α_{eff}. By systematically varying α_{eff} (0.5 and 3.0), the influence of microstructural coupling on soliton dynamics was quantified. The simulations revealed that smaller α_{eff} values (strong coupling) lead to narrower, more localized solitons, while larger α_{eff} values (weak coupling) result in broader soliton profiles due to enhanced dispersion. Despite these changes, the amplitude–velocity relation remained preserved, demonstrating that the internal variable modifies only the dispersive nature of the medium without affecting its nonlinear structure.

The combined results confirmed that the finite volume method is a robust and accurate approach for solving nonlinear dispersive wave equations in both classical and microstructured continua. The method successfully captured the delicate balance between nonlinearity and dispersion, even under modified microstructural conditions. Moreover, the model provides a physically meaningful way to tune dispersion through internal parameters, offering insights into wave localization and dispersion control in structured materials.

Overall, this work contributes to the understanding of nonlinear wave propagation in microstructured solids and establishes a versatile numerical framework that can be extended to higher-dimensional problems, more complex internal variable models, and other classes of nonlinear dispersive equations.

Acknowledgements

I would like to express my sincere gratitude to my supervisor, Professor Arkadi Berezovski, for his continuous guidance, valuable feedback, and encouragement throughout the course of this thesis. His expertise and insightful comments have been essential in shaping the direction and quality of my work. I am truly grateful for the time he dedicated to reviewing my progress and helping me develop a deeper understanding of the subject.

I would also like to thank our study officer, Maarja Märss, and the Dean's Office at the School of Science for their assistance during the administrative process. Their support—especially regarding the procedures for defending my thesis as an external student, important deadlines, and other practical matters—was greatly appreciated.

In addition, I wish to express my appreciation to the authors of the scientific articles, books, and previous theses that I consulted during this work. Their research and publications provided essential ideas, background knowledge, and methodological guidance that helped me develop and complete my thesis.

Finally, I extend my gratitude to the academic staff of the Department of Cybernetics for providing a supportive learning environment throughout my studies.

References

Ablowitz, M. J. and H. Segur (1981). *Solitons and the Inverse Scattering Transform.* Society for Industrial and Applied Mathematics, Philadelphia, PA.

Achenbach, J.D. (1973). *Wave Propagation in Elastic Solids*. North-Holland.

Almatrafi, M.B., Alharbi, A.R. & Tunç, C. (2020). Constructions of the soliton solutions to the good Boussinesq equation. *Advances in Difference Equations, 2020(1), 629*

Berezovski, A. (2011). Thermodynamic interpretation of finite volume algorithms. *Rakenteiden Mekaniikka*, 44(3), 191–204.

Berezovski, A. (2018). Internal variables associated with microstructures in solids. *Mechanics Research Communications,* 93, 30 - 34.

Berezovski, M., Berezovski, A., & Engelbrecht, J. (2010). Waves in materials with microstructure: numerical simulation. *Proceedings of the Estonian Academy of Sciences,* 59(2), 99.

Berezovski, A., Engelbrecht, J., Berezovski, M. (2011). Dispersive wave equations for solids with microstructure. In: Náprstek, J., Horáček, J., Okrouhlík, M., Marvalová, B., Verhulst, F., Sawicki, J. (eds). *Vibration Problems ICOVP 2011: The 10th International Conference on Vibration Problems,* pp. 699-705. Dordrecht: Springer Netherlands,

Berezovski, A., Engelbrecht, J., Salupere, A., Tamm, K., Peets, T., & Berezovski, M. (2013). Dispersive waves in microstructured solids. *International Journal of Solids and Structures*, 50(11–12), 1981-1990.

Berezovski, A. & Ván, P. (2017). *Internal Variables in Thermoelasticity*. Springer, Berlin.

Bona, J.L., Pritchard, W.G., & Scott, L.R. (1985). Numerical schemes for a model for nonlinear dispersive waves, *Journal of Computational Physics,* 60(2), 167-186

Bona, J. L., Chen, M., & Saut, J.-C. (2002). Boussinesq equations and other systems for small amplitude long waves in nonlinear dispersive media. I: Derivation and linear theory, *Journal of Nonlinear Sciences,* 12: 283–318

Christov, C., G. Maugin, and M. Velarde (1996). Well-posed Boussinesq paradigm with purely spatial higher-order derivatives. *Physical Review* E 54(4), 3621.

Debnath, L. (1997). Solitons and the Inverse Scattering Transform. In: *Nonlinear Partial Differential Equations for Scientists and Engineers*. Birkhäuser, Boston, MA.

Drazin, P. G., & Johnson, R. S. (1989). *Solitons: An Introduction.* Cambridge: Cambridge University Press.

Dutykh, D., & Clamond, D. (2016). Modified shallow water equations for significantly varying seabeds. *Applied Mathematical Modelling*, 40(23–24), 9767–9787.

Engelbrecht, J., A. Berezovski, F. Pastrone, and M. Braun (2005). Waves in microstructured materials and dispersion. *Philosophical Magazine* 85(33-35), 4127–4141.

Engelbrecht, J., A. Berezovski, and A. Salupere (2007). Nonlinear deformation waves in solids and dispersion. *Wave Motion* 44(6), 493–500.

Engelbrecht, J., A. Salupere, and K. Tamm (2011). Waves in microstructured solids and the Boussinesq paradigm. *Wave Motion* 48(8), 717–726.

Hirota, R. (1971). Exact solution of the KdV equation for multiple collisions of solitons. *Phys. Rev. Lett.* 27, 1192–1194.

LeVeque, R. J. (1992). *Numerical Methods for Conservation Laws*. 2nd ed. Birkhäuser.

LeVeque, R.J. (2002). *Finite Volume Methods for Hyperbolic Problems*. Cambridge: Cambridge University Press.

Manoranjan, V.S., Mitchell, A.R., & Morris, J.L. (1984). Numerical solutions of the good Boussinesq equation. *SIAM journal on scientific and statistical computing*, 5(4), 946-957.

Maugin, G.A. & Muschik, W. (1994). Thermodynamics with internal variables. Part I. General concepts. *Journal of Non-Equilibrium Thermodynamics.* 19(3), 217-249.

Maugin, G. A. (1999). *Nonlinear Waves in Elastic Crystals*. Oxford University Press

Muschik, W. (1990). Internal variables in non-equilibrium thermodynamics. *Journal of Non-Equilibrium Thermodynamics* 15(2):127-138

Savitzky, A., & Golay, M. J. E. (1964). Smoothing and differentiation of data by simplified least squares procedures. *Analytical Chemistry,* 36(8), 1627–1639.

Sjölander, F. (2021). *Numerical Solutions to the Boussinesq Equation and the Korteweg–de Vries Equation*. KTH Degree Thesis.

Whitham, G. B. (1974). *Linear and Nonlinear Waves.* New York: Wiley–Interscience.

Appendices

Annex
to Rector's directive No 1-8/17 of 7 April 2020

Non-exclusive licence for reproduction and publication of a graduation thesis[1]

I Mohammad Ali Afzal

1. grant Tallinn University of Technology free licence (non-exclusive licence) for my thesis Numerical Solution to Boussinesq-Type Equation in Microstructured Solids,

supervised by Arkadi Berezovski,

1.1 to be reproduced for the purposes of preservation and electronic publication of the graduation thesis, incl. to be entered in the digital collection of the library of Tallinn University of Technology until expiry of the term of copyright;

1.2 to be published via the web of Tallinn University of Technology, incl. to be entered in the digital collection of the library of Tallinn University of Technology until expiry of the term of copyright.

2. I am aware that the author also retains the rights specified in clause 1 of the non-exclusive licence.

3. I confirm that granting the non-exclusive licence does not infringe other persons' intellectual property rights, the rights arising from the Personal Data Protection Act or rights arising from other legislation.

21.12.2025

[1] *The non-exclusive licence is not valid during the validity of access restriction indicated in the student's application for restriction on access to the graduation thesis that has been signed by the school's dean, except in case of the university's right to reproduce the thesis for preservation purposes only. If a graduation thesis is based on the joint creative activity of two or more persons and the co-author(s) has/have not granted, by the set deadline, the student defending his/her graduation thesis consent to reproduce and publish the graduation thesis in compliance with clauses 1.1 and 1.2 of the non-exclusive licence, the non-exclusive license shall not be valid for the period.*